REVIEW OF SCIENTIFIC INSTRUMENTS 76, 033504 (2005)

Active radiometric calorimeter for absolute calibration of radioactive sources

K. E. Stump[a] and L. A. DeWerd
Department of Medical Physics, University of Wisconsin-Madison, Madison, Wisconsin 53706

D. A. Rudman and S. A. Schima
National Institute of Standards and Technology, Boulder, Colorado

(Received 23 November 2004; accepted 12 January 2005; published online 1 March 2005)

This report describes the design and initial noise floor measurements of a radiometric calorimeter designed to measure therapeutic medical radioactive sources. The instrument demonstrates a noise floor of approximately 2 nW. This low noise floor is achieved by using high temperature superconducting (HTS) transition edge sensor (TES) thermometers in a temperature-control feedback loop. This feedback loop will be used to provide absolute source calibrations based upon the electrical substitution method. Other unique features of the calorimeter are (a) its ability to change sources for calibration without disrupting the vacuum of the instrument, and (b) the ability to measure the emitted power of a source in addition to the total contained source power. © *2005 American Institute of Physics.* [DOI: 10.1063/1.1867032]

I. INTRODUCTION

It is estimated that each year in the United States over 220 000 men are diagnosed with prostate cancer.[1] Over the past decade, the number of permanent source implants in the treatment of prostatic carcinoma has increased. This technique is called brachytherapy and has become an important treatment modality for this disease. With this treatment, approximately 100 ^{125}I or ^{103}P sources are permanently implanted inside the prostate gland under the guidance of ultrasound. The entire dose is delivered continuously during source decay, over the period of approximately 1 year. Although the construction of sources varies, in general each source is roughly the shape of a right cylinder with a diameter of 0.8 mm and a length of 4 mm. The outside of the source consists of Ti encapsulation and the internal geometry varies by manufacturer.

One of the fundamental components of successful treatment using permanent source implantation is accurate determination of source strength. The current U.S. standard for source strength for these types of sources has been established at the National Institute of Standards and Technology (NIST) in Gaithersburg, MD. This standard is given in terms of the kinetic energy released in matter (kerma) in air. The specific quantity used for source strength is called the air kerma strength (S_k) and is defined as the air kerma rate times the square of the distance between the source and detector. The units of S_k are cGy cm^2 h^{-1}, where 1 Gray (Gy) is 1 J/kg and 100 cGy=1 Gy. NIST air kerma strength calibrations have a total uncertainty of 3% (coverage factor k=2, which indicates a 2σ uncertainty).

This paper describes the design, construction, and initial characterization of a cryogenic calorimeter designed specifically to provide an absolute measurement of the power deposited by this class of brachytherapy source. The measurement provided by the calorimeter is absolute in that the instrument does not require calibration with a known radiation source. The calorimeter provides a measurement of power in terms of energy per unit time (W) and makes use of the well-established electrical substitution method. This method was developed independently by Kurlbaum in 1892[2] and Ångstrom in 1893.[3] The electrical substitution method has become the method of choice for accurate, high-precision absolute radiometry.[4]

The use of a calorimeter to measure radioactivity is by no means a novel technique. Indeed, one of the first uses of radiometric calorimetry was by Pierre Curie and James Dewar, who constructed a cryogenic calorimeter to probe the nature of the newly discovered phenomenon of radioactivity.[5] Curie and Dewar found that the rate of heat production from a radium sample was the same at cryogenic temperatures as it was at room temperature. Since chemical processes were known to decrease in rate with decreasing temperature, Curie and Dewar were able to postulate that the phenomenon of radioactivity was a fundamental transformation in the atomic structure, not a chemical reaction.

Arguably the greatest achievement in radiometric calorimetry occurred in 1925, when Ellis and Wooster used a calorimeter to demonstrate that there was a difference between the maximum and average energies of the electrons emitted from ^{210}Bi. In 1930, Meitner and Orthmann confirmed this result. This was conclusive evidence that suggested to Pauli the need for the neutrino.[6,7] For an extensive history of the field of radiometric calorimetry, the reader is referred to excellent, if dated, review articles by Gunn[8–10] and Ramthun.[11]

The field of medical radiometric calorimetry has been limited primarily to the calibration of external radiation sources. It is in this area that medical radiometric calorimetry has had its largest impact. The current U.S. absorbed dose to

[a]Electronic mail: kstump@wisc.edu

water standard for ^{60}Co, which is the basis for calibration of medical linear accelerators, is based upon a water calorimeter developed by Domen at the National Bureau of Standards (now NIST).[12] Unfortunately, the techniques that lead to a successful adoption of a calorimetrically based standard for teletherapy sources cannot be extended to brachytherapy sources because a typical brachytherapy source has a power approximately 7 orders of magnitude lower than that of a typical teletherapy source. Thus new approaches must be developed.

To date the most successful calorimeter for the absolute calibration of medical radioactive sources of low energy and low dose rate was developed by Richardson.[13] This calorimeter operated near 8 K and was initially designed to detect the presence of tritium contamination in samples. The instrument made use of a feedback loop similar to the electrical substitution method used here. The initial tests performed by Richardson using electrical heaters in place of radioactive sources indicated that the absolute stability of the calorimeter was 5 μW. Richardson believed that the ultimate stability of the instrument should be better than 0.5 μW. However, that stability has not yet been realized. Richardson's calorimeter was constructed on a partial NIST grant and, after initial testing, it was transferred to NIST in Gaithersburg, MD to undergo initial testing for calibration of β-emitting medical sources. At NIST, the Richardson calorimeter underwent acceptance testing by Collé and Zimmerman.[7] The initial tests were done with ^{90}Sr–^{90}Y and ^{32}P β-emitting brachytherapy sources. The tests found that the short-term stability of the calorimeter (<0.5 d) was about ±1 μW and the long-term stability was on the order of ±5 μW. In addition, uncertainties on the order of 2%–3% were obtainable only by measuring a 25 μW source with several repeated measurements. Collé and Zimmerman described several design flaws and corrections; however, a follow up report has not been issued.

The current calorimeter is designed to provide a more accurate and precise measurement of low-energy, low-power ^{125}I photon-emitting brachytherapy sources than has previously been available. The ultimate goal is to provide an absolute calibration of sources of clinical strength ($\leqslant$1.8 μW). The overall uncertainty of the measurement should be less than 2% (k=2).

II. INSTRUMENT DESIGN

A cross section of the calorimeter described in this report is shown in Fig. 1. The primary goal of the design is to provide a stable platform for the measurement of sources with powers ranging from 0.5 to 10 μW. The criteria for the measurement are that it must be absolute (no external radiation source required for calibration), and as metrologically pure as possible; the total k=2 uncertainty should be below 2%, and multiple measurements of a single source should be possible without disrupting the instrument.

There are numerous thermodynamic advantages to operating the calorimeter at cryogenic temperatures (e.g., lower specific heat and higher thermal conductivity for the radiation absorber material compared to those at ambient temperatures). In addition, operation at low temperature facilitates the adoption of recent advances in absolute radiometry. The most important of these is the use of high temperature superconducting (HTS) transition edge sensors (TES) as thermometers. Thus, the interior of the calorimeter is housed in a custom fabricated liquid nitrogen Dewar. The measurement chamber consists of a stainless steel core with two holes of nominal 1 in. diameter to house the detector assemblies. The end plates of the detector housing are sealed with gaskets of 0.6 mm diameter aluminum wire. The bottom of the detector housing has two holes of nominal 0.75 in. diameter that provide connection to the vacuum system and allow passage of the cables connected to the detector assemblies. The bottom of the custom Dewar has a 6 in. diameter vacuum flange with Conflat-type fittings. The detector housing connects to this fitting with a copper vacuum gasket. The cavity between the walls of the Dewar is thus continuous with the vacuum system, allowing the entire instrument to be evacuated at the same time. The detector assemblies are screwed into the top of the housing. The interior of the detectors are vacuum tight and, therefore, separated from the interior of the housing. The top of the housing has two stainless steel tubes of 0.25 in. diameter inserted in it—one for each of the detector assemblies. These inserts are also vacuum tight. The interiors of these tubes are continuous with the interiors of the detector assemblies. There are therefore two separate vacuum chambers in the instrument. One is the interior of the detector housing (outside of the detectors) and the intrawall cavity of the Dewar. The other is the interior of the detectors and the tubes extending from the top of the detector housing. Having two separate vacuum chambers is necessary to allow sources to be changed without having to vent the entire instrument.

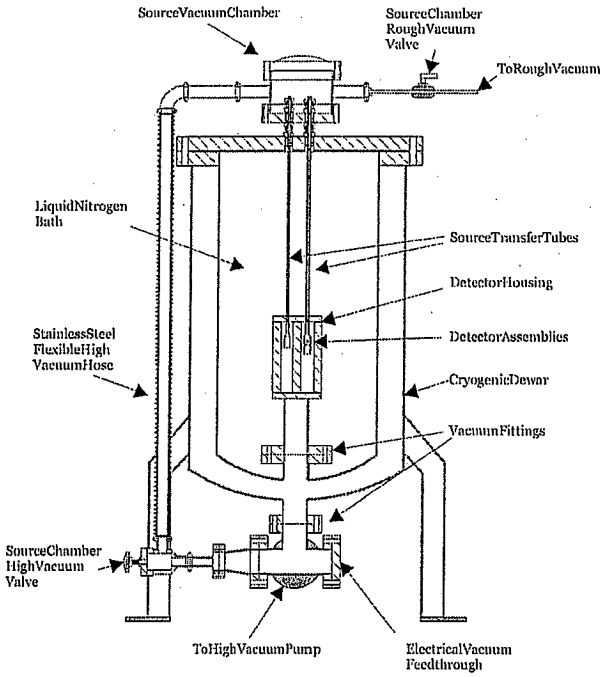

FIG. 1. Scale cross sectional diagram of the calorimeter described in this report.

The vacuum system of the instrument consists of a tur-

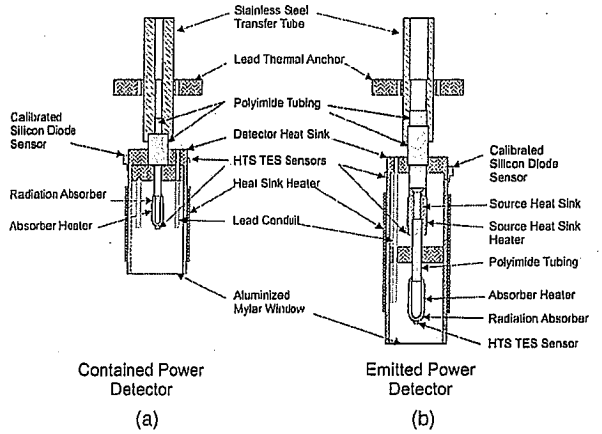

FIG. 2. Scale cross-sectional drawings of the two detectors in the calorimeter. (a) is the detector designed to measure the total contained power. (b) is the detector designed to measure the emitted power of the source.

bomolecular high vacuum pump and a rotary vane pump for the roughing pump. All of the vacuum fittings are stainless steel and use either copper or Viton gaskets. The point of connection between the two vacuum chambers of the calorimeter is controlled by a manual valve. During normal operation the instrument is evacuated to less than 1.3×10^{-4} Pa (1×10^{-6} Torr). However, for the tests described here, the initial weak thermal links between the detector heat sinks and the liquid nitrogen bath were not sufficient to allow proper operation. This was overcome by operating the calorimeter vacuum at 8.0×10^{-3} Pa (6.0×10^{-5} Torr). In the future, this remedy will be replaced by a thermal link that has a heat transfer coefficient large enough to allow operation at high vacuum.

A. Detector design

There are two different detector designs employed by the calorimeter. The first is designed to measure the total contained power of a radioactive source. The total contained power of a source is the total power that is released by radioactive decay. This includes both the power that leaves the source and that which is absorbed by the source itself. The second detector type is designed to measure only the fraction of the power that is emitted by the source, excluding that absorbed by the source. A schematic diagram of both designs is shown in Figs. 2(a) and 2(b).

The radiation absorbers are made of pure 99.995% silver. The wall thickness is sufficient to stop more than 99.999% of the incident radiation for the highest clinically relevant energy present in the sources to be measured by the instrument (the 35.5 keV γ emission of ^{125}I). Extensive Monte Carlo studies have been done for both absorber designs using MCNP4C particle transport code,[14] and the overall efficiency of the absorbers is greater than 99.96%. The 0.04% inefficiency is due predominantly to the open top of the absorbers that allows the source to be transported into and out of the absorber. This is a systematic correction that will have to be applied to the final measurements of the calorimeter.

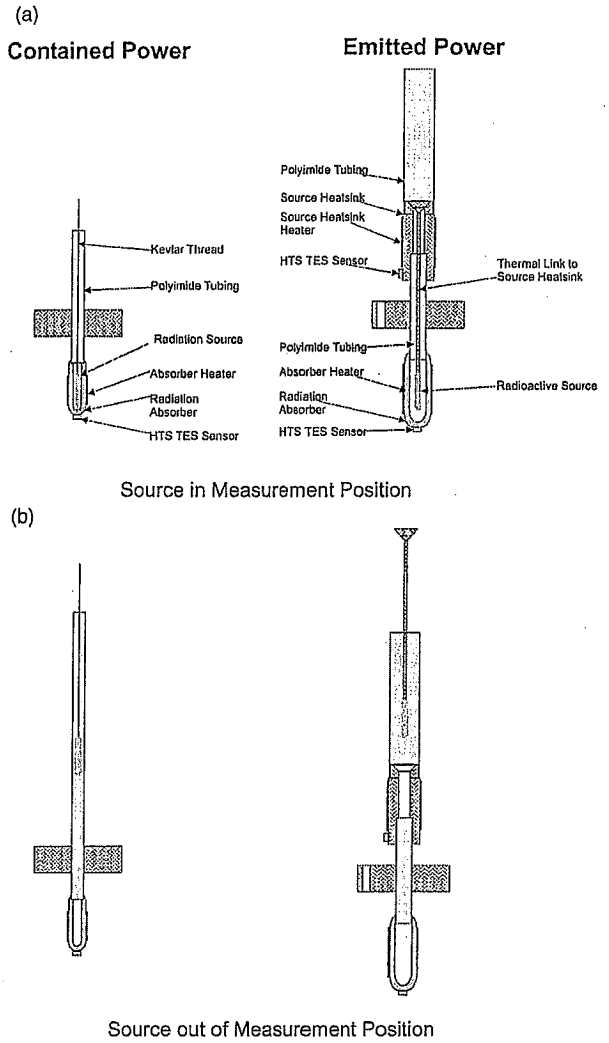

FIG. 3. Scale drawings showing the internal components of both detectors. (a) Shows both detectors with the source in the measurement position. (b) Shows both detectors with the source out of the measurement position.

In both detector designs the absorbers are connected to copper heat sinks by a short length of polyimide tubing. The heat sinks are connected by polyimide tubing to stainless steel transfer tubes. The stainless steel tubes are in direct thermal contact with the liquid nitrogen bath. All bonds are made with Stycast epoxy (2850FT catalyst 9).[15]

The ability to discern emitted versus self-absorbed radiation requires one additional element in the detector design, as seen in Fig. 2(b). Figure 3(a) shows the design of the internal components of both detectors. Figure 3(a) shows the detectors with the source in measurements position, while Fig. 3(b) shows the detectors removed from the detectors, as described in Sec. II B. In order to separate the power that is self-absorbed by the source from that emitted by the source, the radioactive source must be connected to a separate heat sink via a thermal link. This heat sink is labeled "Source Heat Sink " in both Figs. 2(b) and 3. This separate heat sink consists of a copper cylinder that has been machined to interface with the source thermal link when the source is in the measurement position. The source heat sink has a NiCr

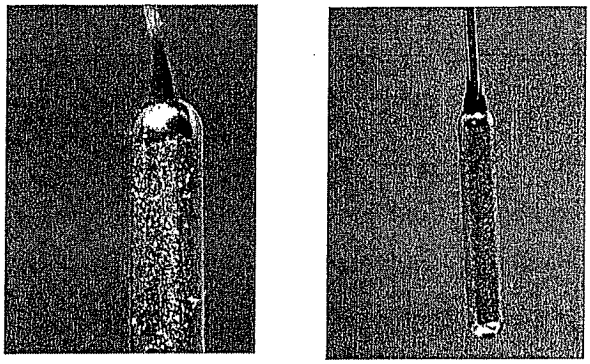

FIG. 4. Photographs showing the source attached to a thread or the source heat sink thermal link.

heater wire and a HTS TES sensor to allow it to be independently temperature controlled. During a measurement, the source heat sink and the radiation absorber are controlled to the same temperature in order to prevent radiative heat transfer. The thermal link between the radioactive source and the source heat sink consists of a copper cone with a stainless steel tube attached to it. Inside the stainless steel tube is a copper wire that conducts the heat from the source to the heat sink. A feature of the design is that both the emitted power and the self-absorbed power are determined independently. The sum of these two values should be equal to the value obtained from the measurement of contained power performed with the contained-power detector shown in Fig. 2(a).

Heaters for each of the heat sinks and absorbers are made by wrapping each element with NiCr wire that has polyimide insulation. The resistance of the heater wires varies from $\approx 32\ \Omega$ for the contained power absorber to $\approx 112\ \Omega$ for the emitted power heat sink.

B. Measurement process

In order to transport the radioactive source into and out of the radiation detectors the source is attached to either a thin kevlar thread (for measurements of contained power) or the source heat sink thermal link (for measurements of emitted power) with a small amount of cryogenic epoxy. Photographs showing a source attached to a thread and the source heat sink thermal link are shown in Fig. 4. The source heat sink thermal link is also attached to a kevlar thread. These threads are wound around bobbins that are placed inside the source vacuum chamber (see Fig. 1) and connected to motors. The source is then lowered into the transfer tubes but not into the detectors.

A source measurement is made by first determining the power required to maintain a constant resistance setpoint for the HTS TES sensors. The sensor used depends upon the measurement being made. If the source's contained power is to be measured, the contained power absorber is controlled. If the emitted power is the measured quantity, both the source heat sink and the emitted power absorber are controlled. Depending whether the self-absorbed power or the emitted power is to be measured, either the power from the source heat sink heater or the power from the emitted power absorber heater is recorded.

Once the power required to maintain the setpoint resistance is determined, the source is lowered into the measurement position. For the measurement of contained power this position is with the source is resting at the bottom of the contained power absorber. For the measurement of emitted power the source heat sink thermal link is engaged with the source heat sink, as shown in Fig. 3. The measured value is then simply the difference between the power measured without the source in the measurement position and the power measured with the source in measurement position. The measurement can be repeated as many times as necessary without disrupting the instrument.

C. Thermometry and temperature control

The key to the calorimeter's operation is low-noise, precise temperature control. The temperature-control scheme used by the calorimeter is designed around the use of HTS TES thermometers. These devices have proved to be very successful in the field of absolute radiometry, where room-temperature systems did not offer sufficient sensitivity, and low-temperature techniques such as infrared radiometry were either not applicable or undesirable.[16]

Typical high-quality HTS TES bolometers exhibit a maximum transition slope on the order of 1000 Ω/K.[16,17] This sensitivity can produce an improvement in noise equivalent power (NEP) by approximately a factor of 100 over that of platinum resistance thermometers operating at liquid nitrogen temperatures.[17] By using HTS TES thermometers, Rice *et al.* determined the noise floor for the NIST Medium Background Infrared (MBIR) Active Cavity Radiometer (ACR) approached 20 nW with a temperature stability of 10 μK.[16] Using a similar design Libonate and Foukal calculated a noise floor of 1.6 nW and a temperature stability of 0.7 μK.[17] Based upon the success these devices have enjoyed in radiometry, they were selected as the thermometers of choice for the calorimeter described here.

The HTS TES thermometers used in the calorimeter were fabricated at NIST-Boulder using the same masks that were developed by Rice for the MBIR ACR. The fabrication technique was similar to that used by Rice.[16,18] The sensors were created on a 500 μm thick $LaAlO_3$ (LAO) substrate. Upon this substrate 120 nm of $YBa_2Cu_3O_{7-\delta}$ (YBCO) was deposited by a laser-ablation process. The YBCO was then covered with 300 nm of gold. Following the deposition, the sensor patterns were produced by a combination of photolithography and ion milling. A single wafer was created and then diced into 1 mm $\times$ 1 mm $\times$ 0.5 mm sensors. Each of the sensors has a thin strip of YBCO with four gold contact pads. The wafer contains 3 different patterns that vary by YBCO strip width. The three widths are nominally 10 μm, 40 μm, and 100 μm. The sensors used by Rice *et al.* had a YBCO film thickness of 80 nm versus the 120 nm used here. Therefore, the current sensors have significantly lower resistance.

Electrical contact is made to the sensors using 76.2 μm diameter copper wire. The lead wires are attached to the gold contact pads with silver-filled epoxy. A photograph of one of

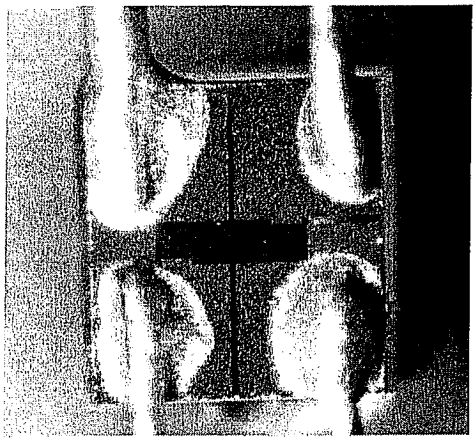

FIG. 5. Photograph of one of the HTS TES thermometers after the copper leads have been attached with silver-filled epoxy.

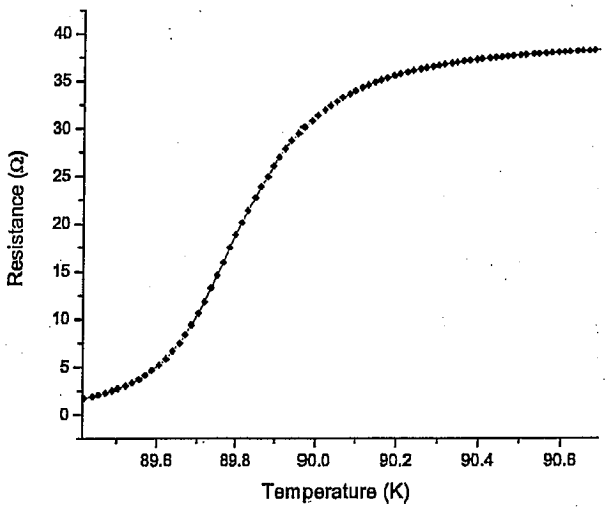

FIG. 6. Typical resistance versus temperature curve for the sensors used in the calorimeter. Note the narrow transition width ~0.3 K.

the sensors after lead attachment is shown in Fig. 5. The copper wires are connected to phosphor-bronze lead wire using silver-filled epoxy after the sensors have been mounted to the detector components using silver-filled epoxy to ensure good thermal contact. The phosphor-bronze lead wire passes through a copper thermal anchor before exiting the detector housing. The phosphor-bronze wires are then connected to a NbTi cryogenic cable which has stainless steel shielding. This cable then runs to one of two electrical vacuum feedthroughs. Outside the Dewar the connections between the feedthroughs and the instrumentation are made by shielded cables.

Temperature control for the calorimeter is achieved by connecting the TES sensors to one of two ac resistance bridges that have temperature control capabilities. The absorber temperatures are controlled by a LakeShore Cryotronics Model 370 AC bridge, and each of the heat sinks is controlled by an individual channel of a Cryo-Con Model 62 bridge.[15] Both bridges have built-in heater outputs that are controlled using a PID control algorithm. The LakeShore bridge can control a single channel while the Cryo-Con bridge can control two channels simultaneously. All of the instruments used in the calorimeter are connected to a PC via a General Purpose Interface Bus (GPIB).

The initial step in the tuning of the control loops was to establish resistance versus temperature curves for all of the TES thermometers. A typical curve for one of the sensors is shown in Fig. 6. The temperature was determined by mounting calibrated silicon diode thermometers to the heat sinks. These sensors are monitored with a LakeShore Cryotronics Model 218 temperature monitor. To generate the curve for the heat sink TESs the heat sink was slowly heated and the temperature and resistance recorded. In order to generate the curves for the absorber and the source heat sink TESs, the heat sinks were temperature controlled to different temperatures for several minutes until the absorbers and source heat sink were able to come to thermal equilibrium. At this point, the resistance of the TES under test was measured and the current temperature was recorded.

Optimal resistance values were selected from the resistance versus temperature curves for the operation of each of the detectors. In each case, the absorber and source heat sink resistances were chosen such that their operating temperature would be slightly higher than that of the heat sinks. This assures that heat will flow from the detector to the heat sink. The control loops for the heat sink TES thermometers were tuned by use of the Zeigler–Nichols frequency tuning method. While there is a vast amount of literature regarding tuning PID controllers, and there are much more sophisticated algorithms, the extreme sensitivity of the detectors to a small change in heater power made dynamic model generation difficult.

The goal for tuning the heat sink loops is to achieve as stable a temperature (process variable) as possible. Stabilizing the process variable is the primary objective for most controllers. As such, a standard tuning procedure was appropriate. For the absorbers, the goal is to minimize the power fluctuations required to maintain a constant temperature. In tuning for a stable control variable (rather than process variable) there is a decrease in response performance.[19] The trade off between fast response time and low power fluctuations can be alleviated somewhat by use of one set of parameters during source insertion and removal to recover quickly from the incident power change and then another different set of parameters once the transients are removed, as was discussed by Reintsema *et al.*[19]

While experimenting with different control coefficients, it quickly became apparent that lower power fluctuations were obtained by use of smaller proportional (P) coefficients. However, use of low values for P has two significant disadvantages. The first is that the system is slow to respond to either setpoint changes or changes in power level, such as occurs during the insertion or removal of a source. The second, and more important disadvantage, is the increase in drift. With small P values, drift is seen in both the heater power and the temperature of the TES. Having a drift in the power is undesirable because drift subtraction must then be performed. Drift in temperature is to be avoided as much as possible because the electrical substitution method presupposes that the radiation source power is the difference in the

heater power required to maintain a constant temperature with and without the source present. Thus, temperature drifts undermine the premise of the method. Therefore, the tuning of the temperature control loops for the radiation absorbers requires a compromise between thermal drift and heater power fluctuations.

Since both temperature controllers used with the calorimeter allow the control parameters to be set remotely, a gain scheduling scheme was adopted. This technique uses parameters that are optimized for a fast response to a disturbance (source insertion or removal). Once the setpoint resistance has been reached and the substitution power stabilized, the control loop parameters are changed to provide a lower level of power fluctuation. The gain schedule goes through two intermediate steps between the fast response and low noise settings. This is done in order to improve the stability of the control loop in the low noise setting. The data presented later in this report are taken with the controllers in the low-fluctuation control mode.

III. HEATER POWER MEASUREMENT

Since the calorimeter uses the electrical substitution method to determine the source power, the primary measurement being made is the absorber heater power. Thus, the measurement is a measure of the amount of power required to maintain a constant absorber temperature both with and without the source in the absorber. The source power is simply the difference between the two power levels. Therefore, great care must be made when measuring the absorber heater power. The power generated by the heater can be determined by monitoring the current through the heater and/or the potential across the heater. The most accurate and reliable method is to measure the current through the heater and the potential across the heater by use of a four-wire technique. The heater power is then given as

$$P = IV, \tag{1}$$

where P is the heater power, I is the current through the heater, and V is the potential across the heater. In order to measure the current, a Keithley model 6517 electrometer is placed in series with the heater. The potential is measured with an Agilent Technologies model 34401A digital multimeter.[15] As with the other instruments, these are connected to a PC using a GPIB.

IV. NOISE CHARACTERIZATION

The objective of the initial phase of testing for the calorimeter is to determine the expected noise floor of the instrument. These characteristics will determine measurement times and the range of source strengths that can be measured. As stated previously, the overall goal of these tests is to minimize the power fluctuations of the absorber heaters. There are several figures of merit that could be used to quantify the noise floor of the instrument. The quantification of the noise in the system depends upon the type of noise present. Noise in metrology is characterized by its spectral composition. The most common characterization is based upon its frequency-domain slope, α. Since the measurement described here is made at near dc, the system will be dominated by $1/f$ noise ($\alpha=-1$). As such, the apropos figure of merit is the Allan variance.[20] As discussed by Reintsema *et al.*, in the presence of $1/f$ noise the classical variance is divergent. This is not the case with the Allan variance. The Allan variance for a discrete series of measurements is computed with the following formula:

$$\sigma_y^2(\tau_0) = \frac{1}{2(N-1)} \sum_{k=1}^{N-1} (y_{k+1} - y_k)^2, \tag{2}$$

where τ_0 is the integration time for each measurement, N is the total number of points collected, and y_k are the time series data points.[19] For a system dominated by low frequency noise, the noise floor is set by the minimum of the Allan variance. For a system comprised entirely of white noise, the Allan variance and the classical variance converge, and the ratio of the classic variance to the Allan variance is unity.[20] This forms a simple test to determine the noise contained in the system and the relevance of the classical variance as a statistical tool.

The minimum of the Allan variance is found after collecting an equally spaced time series of data with N data points. The behavior of σ_y^2 on the integration time can be determined by averaging adjacent data points using the following equation:[20]

$$\sigma_y^2(\tau_0) = \frac{1}{2(N-2n+1)} \sum_{k=1}^{N-2n+1} \left(\frac{1}{n} \sum_{j=k+n}^{k+2n-1} y_j - \frac{1}{n} \sum_{j=k}^{k+n-1} y_j \right)^2. \tag{3}$$

Here $\tau_0 = n\tau_{\min}$, where $\tau_{\min}$ is the minimum averaging time. The values of n are given as $n=2^i$, with $i=0,1,2,\ldots$. Therefore, the minimum of the Allan variance is the smallest value calculated with Eq. (3) for a range of n values.

If the noise of a system has a power-law spectrum, then the Allan variance is proportional to $(\tau_0)^{\mu}$. In the context of the Allan variance, μ is the time-domain power-law dependence.[19] As a result, $\log \sigma(\tau_0) \sim (\mu/2) \log \tau_0$. Thus, insight into the spectral nature of the noise can be gained from a log–log plot of σ_y versus τ_0. The slope of the plot, $\mu/2$, gives information about the spectral type of noise since $\alpha=-(\mu+1)$.

In an effort to guide the tuning process of the temperature control loops, the computer software written to control the calorimeter allows the user to select a region of the power plot and then calculate the minimum Allan variance for that region. Fine tuning the control loops consists of selecting coefficients that minimize the minimum Allan variance for each data set.

V. NOISE FLOOR MEASUREMENT

Once the control loops were properly tuned, the calorimeter could be tested for minimum noise floor, short-term stability, and long-term stability. As discussed above, the reported values are given in terms of the square root of the minimum of the Allan variance or Allan standard deviation, σ_p. Here the subscript p has been substituted to indicate that the measurement is a power measurement. Plotting the Allan

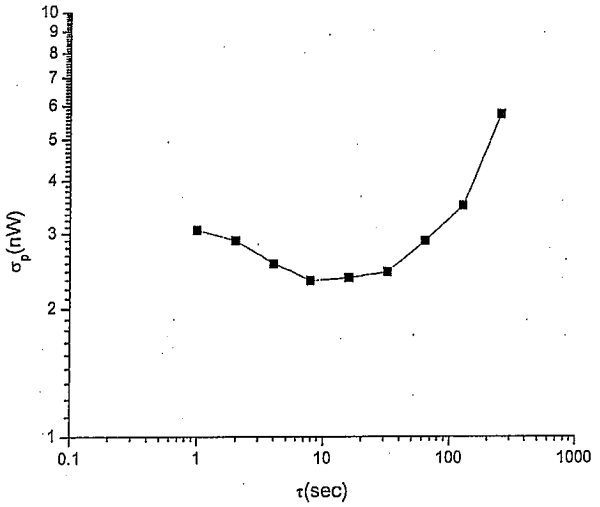

FIG. 7. Square root of the Allan variance plot for a test run of the calorimeter. The plot is a standard σ–τ log–log plot. The data indicate that the optimum integration time for the calorimeter is approximately 8 s.

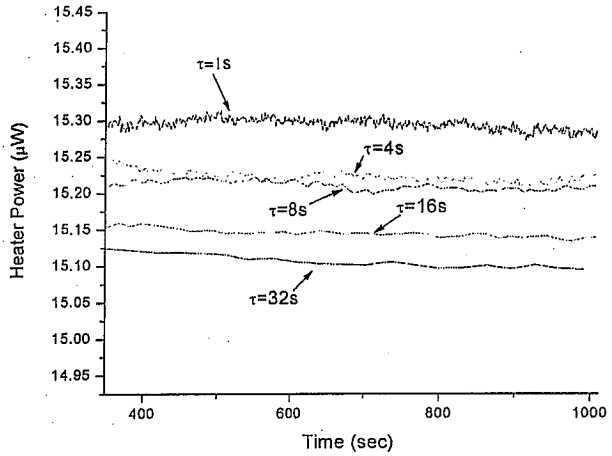

FIG. 9. (Color online) Plot of raw data in the low-noise region of the gain schedule (region 4 of Fig. 8) for different values of integration time τ. The heater powers have been varied slightly to allow better visualization of the data.

standard deviation versus the integration time allows for the estimation of the primary features of the noise power spectrum, provided the spectrum follows a known power law [e.g., $S_p(f) \sim f^{\alpha}$].[19–21]

Figure 7 shows a log–log plot of σ_p vs τ for a time series measurement made with the calorimeter. For $\tau < 8$ s the data are limited by white noise, hence averaging reduces the deviation in the measurements. For integration times longer than 8 s the data are limited by lower-order noise processes. The fact that the minimum of the Allan standard deviation occurs in a region dominated by $1/f$ noise (i.e., $\mu \sim 0$) is consistent with the consensus in the literature that electrical substitution radiometric measurements are dominated by $1/f$ noise, especially in the case that the input is not chopped.

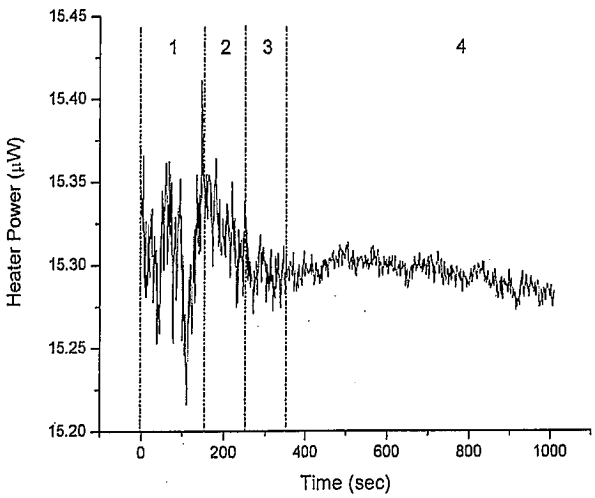

FIG. 8. Plot of the raw power data for the data set used to calculate the minimum of the Allan deviation. The four delineated regions indicate the four different gain scheduling parameters for the control loops. Region 1 is optimized for fast response and region 4 is designed for low noise. Regions 2 and 3 are intermediate optimizations to improve stability.

Several tests were conducted with various substitution powers from 5 μW to 90 μW. The raw data for the data set presented in Fig. 7 are shown in Fig. 8.

A previous section described the gain scheduling scheme employed to reduce drift and improve both the response and the noise of the control loops. In Fig. 8, the different regions of the gain schedule scheme are shown. The first region is optimized for a fast response from a setpoint change or source movement. The second and third regions provide a transition between the fast response and low-noise regions. The fourth region is the low-noise region and is where the final power measurement is made. This method was found to help improve the stability of the measurement in the low-noise parameter setting and reduce thermal drift.

Figure 9 shows raw data from the low-noise region of measurements taken with different integration times, τ. The minimum of the Allan deviation, shown in Fig. 7, predicts that the minimum noise and drift should occur at an integration time of approximately 8 s. This can be seen qualitatively in Fig. 9 as well as the fact that a τ value of 16 s should have a similar amount of noise and drift. The data shown in the figure appear to correspond to the relative noise content predicted by Fig. 7. The classical standard deviation was calculated for the regions shown in Fig. 9 and are listed in Table I. Since the minimum of the Allan variance is 2.3 nW, the data in the table indicate that even at the optimal integration time

TABLE I. Classical standard deviation for the data sets shown in Fig. 9. The Allan deviation for the data sets is 2.3 nW.

τ (s)	σ (nW)
1	27.7
4	7.9
8	6.0
16	6.7
32	9.5

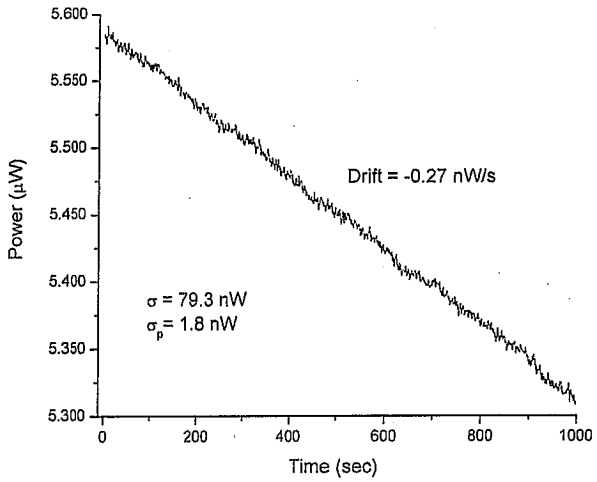

FIG. 10. Raw heater power data taken as the calorimeter slowly warmed. The plot also gives the classical standard deviation, σ, and the Allan deviation, σ_p, for the measurement. The large difference indicates the divergence of the classical variance.

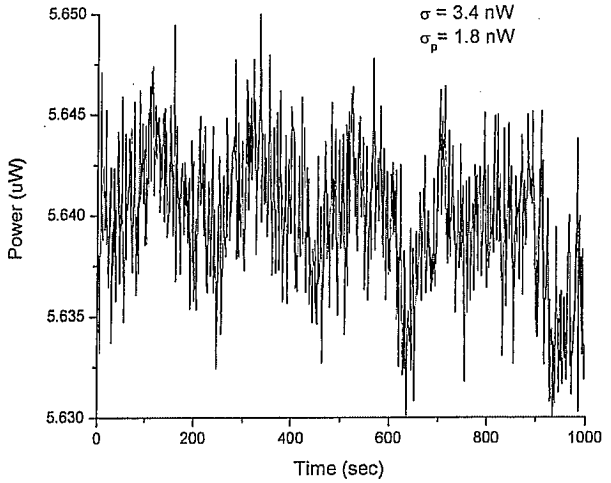

FIG. 11. Plot of the data shown in Fig. 10 with the low-frequency drift subtracted. Again the classical standard deviation for the data set is given in addition to the Allan deviaiton. The removal of the drift causes the two values to converge.

of 8 s, there is still low-frequency noise. The table shows that the classical standard deviation is minimized at the same integration time as the Allan deviation.

A common misconception is that repeating measurements increases the accuracy of the result. Unfortunately, this is true only for systems that contain only uncorrelated, high-frequency noise. As stated earlier, the classical variance diverges in the presence of low-frequency noise. Therefore, in a system containing low-frequency noise repeated measurements can *introduce* noise into the result. In order to demonstrate the relationship between the Allan deviation and the classical standard deviation in the presence of low-frequency noise, measurements were taken as the calorimeter slowly warmed due to low cryogen levels. The raw power data are shown in Fig. 10. This data set is similar to that seen in the radiometer described by Reintsema *et al.*[19] In both cases, the data are dominated by low-frequency drift. In the figure the classical standard deviation, σ, is given in addition to the minimum Allan deviation, σ_p. This demonstrates the divergence of the classical standard deviation in the presence of systematic temperature drift. Figure 11 shows the same data set with the low-frequency drift removed. As was seen by Reintsema *et al.*,[19] the removal of the drift brings the classical standard deviation and the Allan deviation into better agreement.

During the course of the experiments it became clear that the magnitude of the heater power fluctuations decreases with decreasing heater power. For example, the measurement shown in Fig. 8 has an average heater power of 15.295 μW and a minimum Allan deviation of 2.3 nW. For the measurement of the heater power with a large drift component, shown in Fig. 10, the average heater power was 5.640 μW and the minimum Allan deviation was 1.8 nW. Thus the heater power level should be selected to be slightly higher than that of the source under measurement. For both heater power levels the temperature fluctuation over the course of the measurement was less than 13 μK. This is slightly higher than the 10 μK that was reported by Rice *et al.* for the NIST Active Cavity Radiometer.[16]

VI. DISCUSSION

This paper reports the design description and initial testing of a radiometric calorimeter designed to measure the power (both contained and emitted) of medical brachytherapy ^{125}I and ^{103}Pd sources. Prior to this report, the lowest noise of a calorimeter designed to measure this type of source was 5 μW.[7] It should be noted that the noise floor of the instrument reported by Collé and Zimmerman would have been lower had they reported the minimum of the Allan standard deviation. Moreover, the long-term drift and instability issues encountered could have been reduced by using the optimal integration time found by the minimum of the Allan variance. However, it is not likely that the use of the Allan variance as a measure of the instrument noise floor would reduce the figure by 3 orders of magnitude. The calculation of the classical standard deviations presented in Table I does provide a means of direct comparison between the instruments. Thus, the calorimeter described in this report is, to our knowledge, the lowest-noise radiometric calorimeter used to measure low-energy photon-emitting radioactive sources.

It is difficult to compare the results of these tests to those reported by Rice *et al.*[16] since the Rice ACR noise floor was characterized by the root mean square (rms) of the substitution power. However, Rice *et al.* did report that the instrument did not require drift correction, which indicates that there was not a great deal of low-frequency noise. This may have limited the divergence of the classical variance (and therefore the standard deviation). Again the classical deviations presented in Table I can be used to compare the values of the Rice ACR and the current report. That the results of the work of Rice *et al.* and the results presented here are of the same order of magnitude indicates that the two instru-

ments have similar noise characteristics. The 2 nW noise floor reported here is also comparable to the 1.6 nW (rms) reported by Libonate and Foukal for an ACR that was similar in design to that constructed by Rice *et al.* The measurement time was not reported by Libonate and Foukal; however, it is apparent from that report that the data set was collected over approximately 60 s and thus included only relatively high frequency noise. Therefore, the rms should be similar to the square root of the Allan variance.

The only radiometer study that did report the noise floor as the square root of the Allan variance was that of Reintsema *et al.*[19] This radiometer operated at low temperature, ≃9 K, and used Nb TES thermometers. The noise floor for this instrument was approximately 1.2 pW. The much lower noise floor reported by Reintsema *et al.* is to be expected because of the lower operating temperature and the sharper transition edges of the thermometers.

The results of these initial measurements indicate that the calorimeter should be capable of measuring clinical strength brachytherapy sources with an uncertainty of less than about 0.5%. Measurements of radioactive sources are currently being performed, and additional work is being done to determine the total measurement uncertainty. To our knowledge, this is the first report of employing superconducting transition-edge sensors for such a calorimeter.

ACKNOWLEDGMENTS

The authors are grateful to Don McDonald for discussions and advice on radiometer construction and the use of the Allan variance in noise quantification. The authors are also grateful to Gary Frank for his help in the construction of the calorimeter.

[1] American Cancer Society, *Cancer Facts & Figures 2003* (Atlanta, GA, 2003).
[2] F. Kurlbaum, Z. Instrumentenkd. 122 (1893).
[3] K. Ångstrom, Phys. Rev. 1, 365 (1894).
[4] *Absolute Radiometry*, edited by F. Hengstberger (Academic, San Diego, 1989).
[5] P. Curie and J. Dewar, Proc. R. Inst. **17**, 596 (1904).
[6] W. B. Mann, Nucl. Instrum. Methods **112**, 273 (1973).
[7] R. Collé and B. E. Zimmerman Appl. Radiat. Isot. **56**, 1 (2001); **56**, 223 (2001).
[8] S. R. Gunn, Nucl. Instrum. Methods **29**, 1 (1967).
[9] S. R. Gunn, Nucl. Instrum. Methods **85**, 285 (1970).
[10] S. R. Gunn, Nucl. Instrum. Methods **135**, 251 (1976).
[11] H. Ramthun, Nucl. Instrum. Methods **112**, 265 (1973).
[12] S. R. Domen, Med. Phys. **7**, 157 (1980).
[13] J. M. Richardson, IEEE Trans. Nucl. Sci. **47**, 854 (2000).
[14] J. F. Briesmeister, "MCNP—A General Monte Carlo N-Particle Transport Code, Version 4C," Report LA-13709-M, Los Alamos National Laboratory, April 2000.
[15] Manufactures and/or model numbers are identified only for purposes of complete technical description; neither NIST nor the University of Wisconsin Accredited Dosimetry Calibration Laboratory endorse the use of any particular product, and other products may be found to serve just as well.
[16] J. Rice, S. Lorentz, R. Dalta, L. Vale, D. Rudman, M. L. C. Sing, and D. Robbes, Metrologia **35**, 289 (1998).
[17] S. Libonate and P. Foukal, Metrologia **37**, 369 (2000).
[18] F. Stork, J. Beall, A. Roshko, D. DeGroot, D. Rudman, R. Ono, and J. Krupka, IEEE Trans. Appl. Supercond. **7**, 1921 (1997).
[19] C. Reintsema, J. Koch, and E. Grossman, Rev. Sci. Instrum. **69**, 152 (1998).
[20] D. Allan, IEEE Trans. Instrum. Meas. **IM-36**, 646 (1987).
[21] C. Greenhall, IEEE Trans. Instrum. Meas. **47**, 623 (1998).